Continuum Mech. Thermodyn. (2016) 28:561–577
DOI 10.1007/s00161-015-0464-z

ORIGINAL ARTICLE

T. Ahamed · M. B. Rubin · B. A. Trimmer · L. Dorfmann

Time-dependent behavior of passive skeletal muscle

Received: 31 January 2015 / Accepted: 12 July 2015 / Published online: 26 July 2015

Abstract An isotropic three-dimensional nonlinear viscoelastic model is developed to simulate the time-dependent behavior of passive skeletal muscle. The development of the model is stimulated by experimental data that characterize the response during simple uniaxial stress cyclic loading and unloading. Of particular interest is the rate-dependent response, the recovery of muscle properties from the preconditioned to the unconditioned state and stress relaxation at constant stretch during loading and unloading. The model considers the material to be a composite of a nonlinear hyperelastic component in parallel with a nonlinear dissipative component. The strain energy and the corresponding stress measures are separated additively into hyperelastic and dissipative parts. In contrast to standard nonlinear inelastic models, here the dissipative component is modeled using an evolution equation that combines rate-independent and rate-dependent responses smoothly with no finite elastic range. Large deformation evolution equations for the distortional deformations in the elastic and in the dissipative component are presented. A robust, strongly objective numerical integration algorithm is used to model rate-dependent and rate-independent inelastic responses. The constitutive formulation is specialized to simulate the experimental data. The nonlinear viscoelastic model accurately represents the time-dependent passive response of skeletal muscle.

Keywords Passive muscle · Finite deformation · Rate-dependent response · Stress relaxation

1 Introduction

Mathematical and numerical modeling of bioactive materials requires the use of constitutive equations, which in their simplest form must account for the passive, active and transitioning states [1–3]. The challenge is to select or develop an appropriate constitutive law and to experimentally determine the values of associated model parameters. In this paper, the biological model, *Manduca sexta*, is used to examine the time-dependent mechanical properties of the ventral interior lateral muscle (VIL) of the third abdominal segment (A3) under passive conditions. Attention is focused on the A3 VIL skeletal muscle since it is one of the largest larval muscles comprising 14 muscle fibers [4]. Time-independent data of the passive and active states are given in

Communicated by Victor Eremeyev, Peter Schiavone and Francesco dell'Isola.

T. Ahamed · L. Dorfmann (✉)
Department of Civil and Environmental Engineering, Tufts University, Medford, MA, USA
E-mail: luis.dorfmann@tufts.edu

M. B. Rubin
Faculty of Mechanical Engineering, Technion-Israel Institute of Technology, Haifa, Israel

B. A. Trimmer
Department of Biology, Tufts University, Medford, MA, USA

Dorfmann et al. [4], and the transitioning state is discussed in Paetsch et al. [1]. A general representation of the theory of time-dependent materials is given by, for example, Wineman and Rajagopal [5] and Christensen [6].

Unlike either amorphous or crystalline materials, muscles are complex composites. Each muscle fiber contains aligned actin and myosin filaments within an amorphous matrix material composed of proteins, lipids and polysaccharides. Many studies focus on the active state; however, there is a growing appreciation of the importance of the passive properties of these materials for their roles as brakes and dampers.

An outstanding issue in muscle properties is the mechanism by which passive force changes with the deformation rate and how they recover after unloading [7,8]. Different molecular mechanisms are responsible for these time-dependent processes. Both actin/myosin cross-bridge breakage and reformation, and the unfolding of gap-filament proteins (e.g., titin) have been proposed as likely mechanisms [9–13]. Intramuscular collagenous structural elements [14] and muscle junctions [15] may also contribute to properties observed in experimental muscle preparations. At the molecular level, active force production is generated through conformational changes in proteins (specifically myosin heads) and the making and breaking of chemical bonds between aligned proteins. Thus, active shortening is produced by enzymatic processes that consume the chemical energy of phosphate bonds in ATP, a process that even occurs at low levels in inactive muscle and contributes to energy loses. Muscles cannot reverse this metabolic process directly, so the muscle must be re-lengthened by external forces. Re-lengthening involves another structural rearrangement of the protein complexes that contribute to the dissipation of mechanical energy during strain cycling. Both the shortening and lengthening appear to have rate-dependent and rate-independent components as a result of the hierarchical cascade of molecular and mechanical interactions [16]. The distribution of mechanical stresses by each of the components is complex and poorly understood [17,18], but the goal of this paper is to develop a model that better accounts for the overall time-dependent properties of passive muscle. These different molecular mechanisms are important because they influence the assumptions and validity of most mechanical models used to describe muscle behavior.

A seminal contribution to characterize viscoelasticity of skeletal muscle is due to Hill [19]. His experimental data showed that the amount of damping depends on the speed of shortening, conversely on the speed of lengthening. They are used by Hill [19] to define a phenomenological approach to describe the muscle force and force velocity relationships. Hill's two-component model consists of an undamped, purely elastic element in series with an energy dissipating element. The classic two-component model is arranged parallel to a purely elastic spring element, which provides the time-independent response and is known as the three-element Hill's model. Hill's model has been extended to formulate three-dimensional stress–strain formulations, see, for example, Martins et al. [20], Parente et al. [21], Tang et al. [22].

Limited amount of data is available that characterize the viscoelastic properties of skeletal muscles [23,24]. Meyer et al. [25] characterize stress relaxation of single passive muscle fibers and propose a three-element Hill's model to simulate the observed response. The viscoelastic properties of passive skeletal muscle are investigated in Rehorn et al. [26]. Specifically, the change of the passive properties of single muscle fibers as a function of the lengthening velocity is evaluated. The data are then used to develop a uniaxial, quasi-linear viscoelastic model with the relaxation function expressed as a three-term Prony series. The authors attribute the viscoelastic behavior during tensile loading to the passive properties of the protein titan.

Experimental data and finite element modeling of passive rat tibias anterior muscle during compressive loading are given in Bosboom et al. [27]. A one-term Ogden model combined with a Prony series expansion is used to account for the viscoelastic behavior. More recently, the nonlinear anisotropic properties of passive skeletal muscle have been addressed in Van Loocke et al. [28]. Attention is placed on the unconfined compressive behavior of porcine, bovine and ovine muscle samples. A strain-dependent Young's modulus is included in the model to account for the nonlinear behavior. Experimental characterization and a quasi-linear viscoelastic model of muscle tissue in compression is given in Van Loocke et al. [24]. Specifically, the model by Van Loocke et al. [28] is extended by introducing a relaxation function with the viscoelastic properties being transversely isotropic. The behavior of passive skeletal porcine muscle during cyclic compressive loading at different loading rates is characterized in Van Loocke et al. [29], and a nonlinear viscoelastic model to simulate this behavior is given.

Three-dimensional constitutive formulations of skeletal muscles using nonlinear solid mechanics have recently been developed. A hyperelastic, incompressible and transversely isotropic formulation to model the passive and active responses of the left and right masseter muscles is proposed by Röhrle and Pullan [30]. The model given by Ito et al. [31] accounts for viscoelasticity, material anisotropy, damage and failure due to excessive stretch. It is validated in uniaxial tension and compression by comparing numerical results

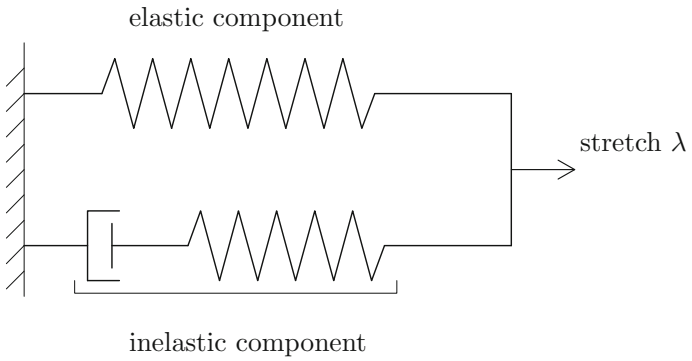

Fig. 1 Schematic representation of the model

to experimental data. An energy function comprised of an isochoric neo-Hookean part combined with an additional fiber contribution is used in [32] to characterize the behavior under tensile load. The fiber response is described using Hill's three-element formulation. A finite-strain anisotropic constitutive law to describe the viscoelastic response of abdominal rat muscles in the passive state is proposed by Calvo et al. [33]. A decoupled volumetric-isochoric representation of the energy function, augmented by an inelastic contribution expressed in terms of internal variables, is used to account for the nonlinear viscoelastic response of muscles in the anterior abdominal wall.

In previous work [4,34], stress–strain relations for loading and unloading of transversely isotropic passive and active muscles were developed using the theory of hyperelasticity. The theory has been modified to account for the hysteretic response of a preconditioned muscle during loading–unloading. Phenomenological relations were included in the model to account for the molecular mechanisms responsible for energy dissipation and rate-dependent material behavior. The pseudo-elastic model in Dorfmann et al. [4,34] did not account for the viscoelastic stress relaxation during loading and the time-dependent recovery at constant elongation from the preconditioned to the unconditioned state.

The objective of this paper is to develop a three-dimensional constitutive model that accounts for the time-dependent behavior of skeletal muscle in the passive state. Hunter et al. [35] model the passive response of cardiac muscle using a hyperelastic orthotropic strain energy function and the incompressibility constraint. In particular, the response to uniaxial stress in the principal directions of orthotropy is consistent with that of an incompressible isotropic material, but with different responses for each direction. In this paper, attention is limited to uniaxial stress in the muscle fiber direction, so it is sufficient to use an isotropic model. Experimental data are used to justify the formulation and to validate the implementation of the numerical integration algorithm. The model considers the material to be a composite of a nonlinear hyperelastic component in parallel with a nonlinear dissipative component (see Fig. 1). Standard models of viscoelasticity are typically formulated in terms of hereditary integrals of the history of deformation and rate of deformation. In contrast, here the dissipative component is based on the model by Hollenstein et al. [36], which exhibits smooth behavior and can be considered as a generalization of a viscoplastic overstress model [37], a generalized plasticity model [38,39] and a generalized hyperplastic model [40]. Specifically, the dissipative component used here models combined rate-independent and rate-dependent inelastic responses with no finite elastic range.

An outline of the paper is as follows. Section 2 presents experimental data of unstimulated *Manduca* muscle subject to simple uniaxial tension. The data quantify the rate-dependent response, the recovery of muscle properties from the preconditioned state toward the unconditioned state and stress relaxation at constant stretch during loading and unloading. Section 3 summarizes the kinematics of finite deformation, the theories of hyperelasticity and rate-dependent and rate-independent inelasticity. Section 4 describes a robust, strongly objective numerical integration algorithm. Then, in Sect. 5, the general framework is specialized to soft tissue that experience large distortional deformations and exhibit exponential stiffening when loaded in tension. In Sect. 6, the model developed is formulated to simulate experimental data in simple uniaxial tension and the corresponding numerical results are included in Sect. 7.

2 Experimental results

Experimental data of the rate-dependent response of an unstimulated muscle of *Manduca sexta* for stretch rates of $\dot{\lambda} = 0.0144, 0.072, 0.36$ and $1.8\ s^{-1}$ are summarized in Dorfmann et al. [34]. The data were used to formulate a pseudo-elastic constitutive model for the mechanical response of the *Manduca* muscle at finite strains. The model accounts for the energy dissipated with each loading–unloading cycle but does not address the effect of recovery time during which a preconditioned muscle returns to the reference configuration upon unloading [34]. In this paper, the rate-dependent response of this material is revisited and a systematic evaluation of time-dependent processes is presented.

During each of the tests, the unstimulated muscle was subjected to five cycles of preconditioning with constant strain rate $\dot{\lambda}$ up to a preselected extension with stretch $\lambda = 1.24$. The experiments started at the prestressed resting length (denoted by point A in Fig. 2), and cycles of loading to point B and unloading to point C were performed at different rates of stretch. The resting length of the muscle, equal to the initial distance of the pinned connections at each end of the muscle, was found to be 5.5 mm and used to determine the corresponding prestressed resting stretch $\lambda_r = 1.05$. Changes in the distance between these connections were measured with an accuracy of 1 μm. The tensile force was measured using an Aurora 300B-LR lever-arm ergometer with an accuracy of less than 0.3 mN. Finally, following the methods summarized in Dorfmann et al. [34], the reference cross-sectional area was found to be $0.4\ mm^2$. This information was used to determine the nominal stress as the ratio of the axial force to the reference cross-sectional area. Preconditioning was performed in order to monitor the progression of stress softening and to determine the ultimate stress–deformation response for stretches up to $\lambda = 1.24$. Figure 2 shows the nominal stress versus stretch λ for the muscle in an unstimulated state with stretch rates of $\dot{\lambda} = 0.0144, 0.072, 0.36$ and $1.8\ s^{-1}$. The data show dependence on the loading rate, large nonlinear elastic deformations, a hysteretic response during loading–unloading and preconditioning (stress softening) during the first few cycles of repeated loading. Recovery, during which the stress increased toward the prestressed resting state, was observed when the muscle was left at its resting length for several minutes. The results in Fig. 2 also show that the reference configuration, corresponding to the resting length of the animal, is not stress-free.

To quantify the recovery of muscle properties from the preconditioned state toward the prestressed resting state, simple uniaxial tension tests were performed on two muscles with a resting length of 4.5 mm and a cross-sectional area of $0.265\,mm^2$. For each test, a total of three loading–unloading cycles were performed from the prestressed resting stretch $\lambda_r = 1.05$ to a maximum stretch $\lambda = 1.24$ at a constant strain rate of $\dot{\lambda} = 0.18\ s^{-1}$. At the end of each loading–unloading cycle, the muscles were held at the resting length for 3 minutes to allow recovery toward the prestressed resting state. The data in Fig. 3 show that the muscles at resting length are not stress-free and that almost complete recovery occurs during the three-minute intervals. Preconditioning occurs, which is noted when the first and second loading paths are compared.

To evaluate stress relaxation, simple uniaxial tension tests were performed on two muscle specimens having a resting length of 4.5 mm and a cross-sectional area of $0.265\,mm^2$. For each muscle, stress-deformation data of a single loading–unloading cycle with constant strain rate $\dot{\lambda} = 0.2\ s^{-1}$ and with maximum elongation $\lambda = 1.26$ were collected. During both the loading and unloading portions of the cycle, interrupted relaxation tests were performed by holding the stretch constant ($\dot{\lambda} = 0$) for 30 seconds at the stretches $\lambda = 1.12$ and $\lambda = 1.19$. The data in Fig. 4 show that the stress decreases during the relaxation tests from the loading portion of the cycle and that recovery with increasing stress occurs during the relaxation tests from the unloading portion of the cycle. Notice that the values of stress after relaxation from the loading portion of the cycle do not equal the values of stress after recovery from the unloading portion of the cycle for the same value of λ. It is not known whether these values of stress would coincide for the same values of λ if more time were allowed for the relaxation tests (as suggested by the model discussed in the next section).

The data reported in this section will be used to formulate a constitutive model for the time-dependent response of the *Manduca* muscle at finite strain. The theory of hyperelasticity is used to characterize the elastic response and a dissipative component to account for the inelastic response of the material. For simplicity, it is assumed that stress relaxation at constant stretch during loading and during unloading approaches the same equilibrium state.

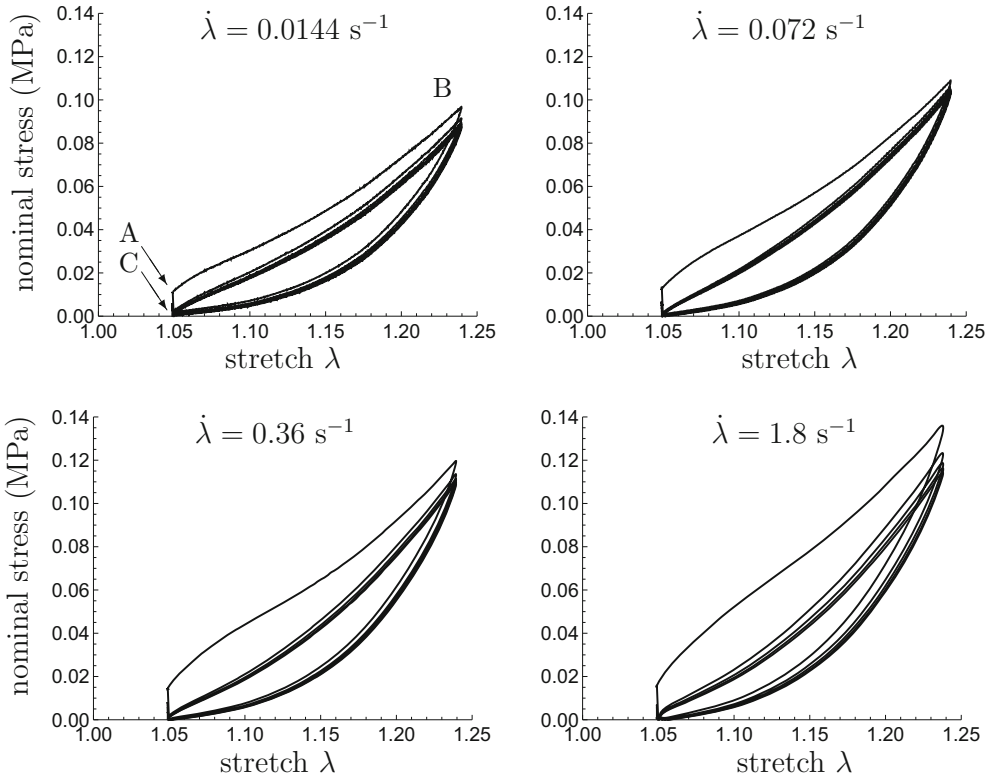

Fig. 2 The nominal stress versus stretch of a passive *Manduca* muscle in simple uniaxial tension with prestressed resting stretch $\lambda_r = 1.05$, maximum extension $\lambda = 1.24$ and stretch rates of $\dot{\lambda} = 0.0144\ \mathrm{s}^{-1}$, $\dot{\lambda} = 0.072\ \mathrm{s}^{-1}$, $\dot{\lambda} = 0.36\ \mathrm{s}^{-1}$ and $\dot{\lambda} = 1.8\ \mathrm{s}^{-1}$. Reproduced from [34]

3 Constitutive modeling

The data in Figs. 2, 3 and 4 suggest that the mechanical behavior of the material can be characterized by a composite model of an elastic component in parallel with a dissipative component. This model is shown schematically in Fig. 1 where the single elastic spring represents the time-independent nonlinear hyperelastic component and the spring element in series with a dashpot represents a nonlinear inelastic response similar to a Maxwell element. In the model discussed below, the dashpot is generalized to include both rate-dependent and rate-independent inelastic responses. Since soft biological tissues undergo finite deformations, the model is formulated for arbitrarily large deformations.

By way of background, it is recalled that a material point in a fixed reference configuration is located by the vector $\mathbf{X}$ relative to a fixed origin. The same material point is located by the vector $\mathbf{x}$ (relative to the same origin) in the present configuration at time t. The velocity $\mathbf{v}$, velocity gradient $\mathbf{L}$ and the rate of deformation tensor $\mathbf{D}$ are defined by

$$\mathbf{v} = \dot{\mathbf{x}}, \quad \mathbf{L} = \frac{\partial \mathbf{v}}{\partial \mathbf{x}}, \quad \mathbf{D} = \frac{1}{2}\left(\mathbf{L} + \mathbf{L}^{\mathrm{T}}\right), \tag{1}$$

where a superposed $(\dot{})$ denotes material time differentiation holding $\mathbf{X}$ fixed. Since the proposed model includes hysteretic dissipation, it is also recalled that the rate of material dissipation $\mathscr{D}$ can be expressed in the form

$$\mathscr{D} = \boldsymbol{\sigma} \cdot \mathbf{D} - \rho \dot{\Sigma} \geqslant 0, \tag{2}$$

where $\boldsymbol{\sigma}$ is the Cauchy stress, $\mathbf{A} \cdot \mathbf{B} = \mathrm{tr}\left(\mathbf{A}\mathbf{B}^{\mathrm{T}}\right)$ denotes the inner product between two second-order tensors $\{\mathbf{A}, \mathbf{B}\}$, ρ is the current mass density, and Σ is the strain energy per unit mass.

Specifically, for the composite model the strain energy is separated additively into a hyperelastic part Σ_e and a dissipative part Σ_d

$$\Sigma = \Sigma_e + \Sigma_d, \tag{3}$$

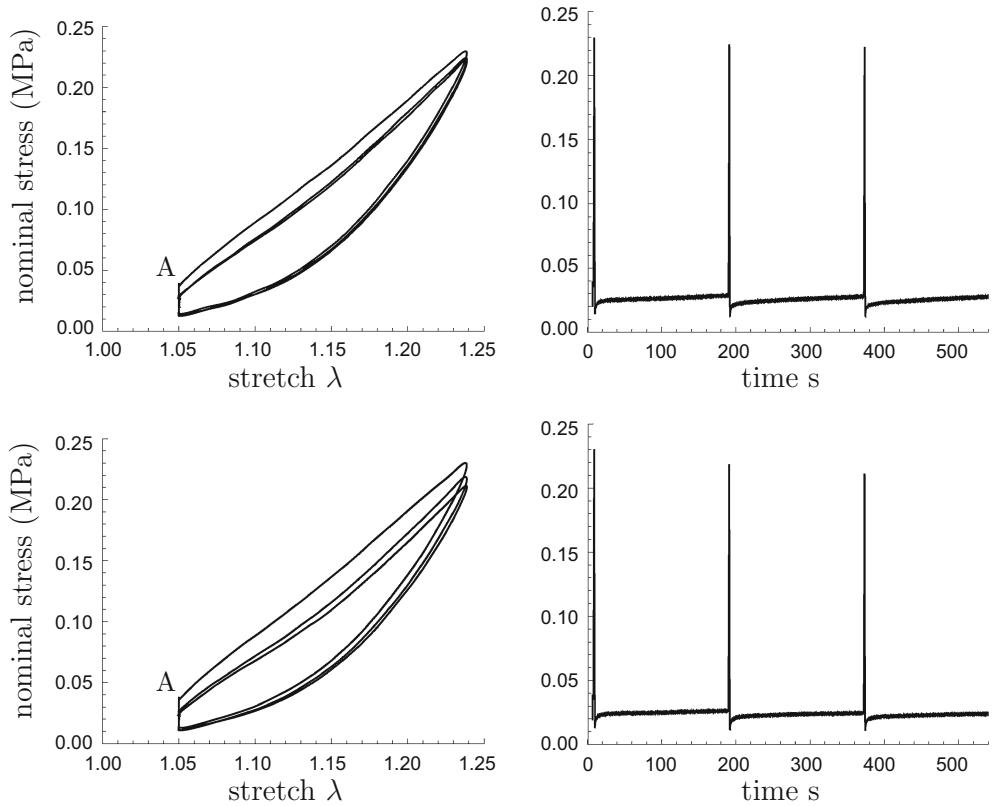

Fig. 3 The stress-deformation responses of two unstimulated muscles in simple uniaxial tension during three loading–unloading cycles. At the end of each unloading, the muscles are held at the resting length for 3 min during which recovery occurs from the preconditioned state to the prestressed resting state (point A). The *left graphs* show the nominal stress as a function of the stretch λ. The graphs on the *right* show the nominal stress as a function of time

where the latter characterizes the elastic strain energy in the dissipative element. Similarly, the Cauchy stress $\boldsymbol{\sigma}$ separates additively into a hyperelastic part $\boldsymbol{\sigma}_{\mathrm{e}}$ and a dissipative part $\boldsymbol{\sigma}_{\mathrm{d}}$

$$\boldsymbol{\sigma} = \boldsymbol{\sigma}_{\mathrm{e}} + \boldsymbol{\sigma}_{\mathrm{d}}, \tag{4}$$

with the hyperelastic component being nondissipative such that

$$\boldsymbol{\sigma}_{\mathrm{e}} \cdot \mathbf{D} = \rho \dot{\Sigma}_{\mathrm{e}}. \tag{5}$$

It then follows that the rate of material dissipation is due solely to the dissipative component which must satisfy the restriction

$$\mathscr{D} = \boldsymbol{\sigma}_{\mathrm{d}} \cdot \mathbf{D} - \rho \dot{\Sigma}_{\mathrm{d}} \geqslant 0. \tag{6}$$

3.1 Hyperelastic component

In general, hyperelastic materials experience both volumetric and distortional deformations. The volumetric deformation is characterized by the total dilatation J, which is determined by integrating the evolution equation

$$\dot{J} = J\mathbf{D} \cdot \mathbf{I}, \tag{7}$$

where $\mathbf{I}$ is the second-order unit tensor. Using the theories in Flory [41] and Ogden [42] it is possible to define a symmetric second-order unimodular tensor $\mathbf{B}'$ which is a pure measure of total distortional deformation by integrating the evolution equation

$$\dot{\mathbf{B}}' = \mathbf{L}\mathbf{B}' + \mathbf{B}'\mathbf{L}^{\mathrm{T}} - \frac{2}{3}(\mathbf{D} \cdot \mathbf{I})\,\mathbf{B}'. \tag{8}$$

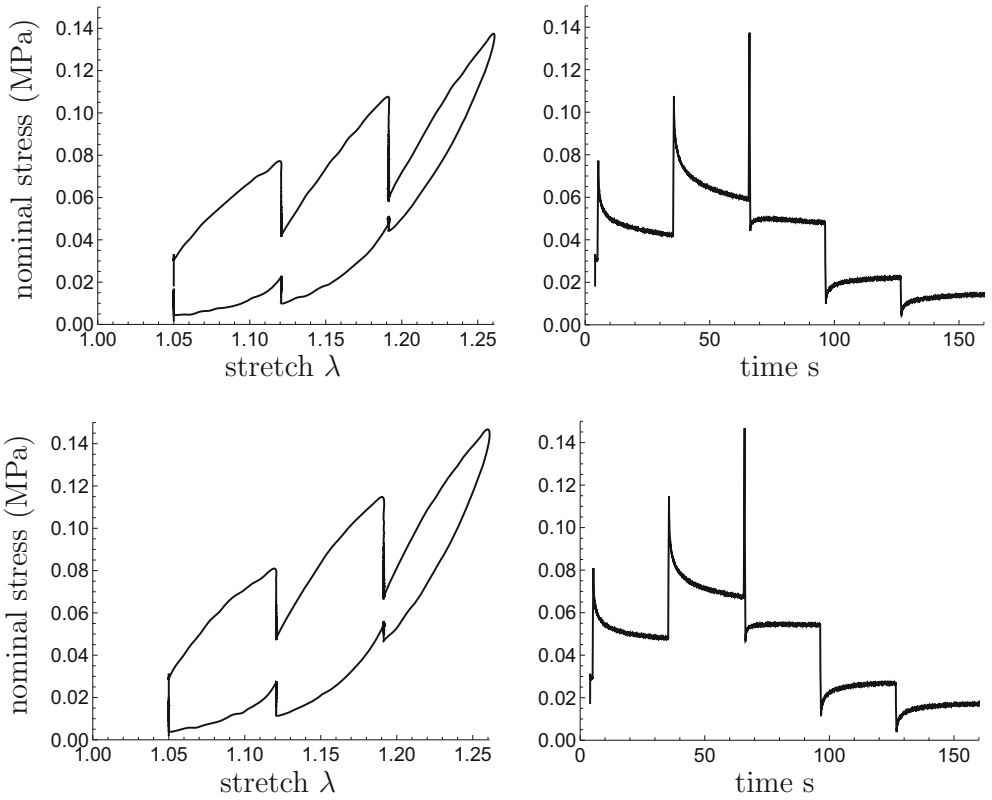

Fig. 4 Experimental data showing the mechanical responses of two unstimulated muscles in simple uniaxial tension during loading and unloading. The graphs on the *left* show the nominal stress versus stretch λ. The graphs on the *right* depict the nominal stress versus time

It can easily be shown that $\mathbf{B}'$ is the unimodular part of the standard left Cauchy-Green deformation tensor. Since $\mathbf{B}'$ is unimodular [$\det(\mathbf{B}') = 1$], it has only two independent invariants. These can be specified by the scalars β_1 and β_2 defined by

$$\beta_1 = \mathbf{B}' \cdot \mathbf{I}, \quad \beta_2 = \mathbf{B}'^2 \cdot \mathbf{I}, \tag{9}$$

which satisfy the equations

$$\dot{\beta}_1 = 2\,\mathrm{dev}\,(\mathbf{B}') \cdot \mathbf{D}, \quad \dot{\beta}_2 = 4\,\mathrm{dev}\,(\mathbf{B}'^2) \cdot \mathbf{D}, \tag{10}$$

where the deviatoric operator dev ( ) of a second-order tensor $\mathbf{A}$ is defined by

$$\mathrm{dev}\,(\mathbf{A}) = \mathbf{A} - \frac{1}{3}(\mathbf{A} \cdot \mathbf{I})\,\mathbf{I}. \tag{11}$$

For elastically isotropic materials the strain energy Σ_e is a function of the invariants $\{J, \beta_1, \beta_2\}$ expressed as

$$\Sigma_\mathrm{e} = \Sigma_\mathrm{e}(J, \beta_1, \beta_2). \tag{12}$$

The hyperelastic part $\boldsymbol{\sigma}_\mathrm{e}$ of the Cauchy stress is then given by

$$\boldsymbol{\sigma}_\mathrm{e} = -p_\mathrm{e}\mathbf{I} + \mathrm{dev}\,(\boldsymbol{\sigma}_\mathrm{e}), \quad p_\mathrm{e} = -\rho_0 \frac{\partial \Sigma_\mathrm{e}}{\partial J}, \tag{13}$$

$$\mathrm{dev}\,(\boldsymbol{\sigma}_\mathrm{e}) = 2\rho \frac{\partial \Sigma_\mathrm{e}}{\partial \beta_1} \mathrm{dev}\,(\mathbf{B}') + 4\rho \frac{\partial \Sigma_\mathrm{e}}{\partial \beta_2} \mathrm{dev}\,(\mathbf{B}'^2), \tag{14}$$

where use has been made of the conservation of mass which connects the mass density ρ in the present configuration to its value ρ_0 in the reference configuration

$$\rho J = \rho_0. \tag{15}$$

3.2 Dissipative component

The work in Rubin and Attia [43] proposes that the elastic distortional deformation of the dissipative component, which is insensitive to volume changes, can be characterized by the symmetric unimodular tensor $\mathbf{B}'_{\mathrm{d}}$, which is determined by integrating the evolution equation

$$\dot{\mathbf{B}}'_{\mathrm{d}} = \mathbf{L}\mathbf{B}'_{\mathrm{d}} + \mathbf{B}'_{\mathrm{d}}\mathbf{L}^{\mathrm{T}} - \frac{2}{3}\left(\mathbf{D}\cdot\mathbf{I}\right)\mathbf{B}'_{\mathrm{d}} - \Gamma\mathbf{A}_{\mathrm{d}}, \tag{16}$$

where the function Γ controls the rate of inelastic distortional deformation and is specified by a constitutive equation. Its direction is controlled by $\mathbf{A}_{\mathrm{d}}$, which is given by

$$\mathbf{A}_{\mathrm{d}} = \mathbf{B}'_{\mathrm{d}} - \left(\frac{3}{\mathbf{B}'^{-1}_{\mathrm{d}}\cdot\mathbf{I}}\right)\mathbf{I}, \quad \mathbf{A}_{\mathrm{d}}\cdot\mathbf{B}'^{-1}_{\mathrm{d}} = 0. \tag{17}$$

This functional form for $\mathbf{A}_{\mathrm{d}}$ causes inelastic relaxation of $\mathbf{B}'_{\mathrm{d}}$ toward the unit tensor $\mathbf{I}$, with the restriction $(17)_2$, ensuring that $\mathbf{B}'_{\mathrm{d}}$ remains unimodular. Moreover, comparison of (16) with (8) shows that when the rate of inelasticity $\Gamma\mathbf{A}_{\mathrm{d}}$ vanishes, $\mathbf{B}'_{\mathrm{d}}$ satisfies the same evolution equation as that for the total elastic distortional deformation $\mathbf{B}'$. However, $\mathbf{B}'_{\mathrm{d}}$ can still differ from $\mathbf{B}'$ if the material experienced any inelastic deformation during its history of loading, since $\mathbf{B}'_{\mathrm{d}}$ does not retain permanent memory of a specific reference configuration.

Two independent invariants of $\mathbf{B}'_{\mathrm{d}}$ can be specified by the scalars $\{\alpha_1, \alpha_2\}$ as

$$\alpha_1 = \mathbf{B}'_{\mathrm{d}}\cdot\mathbf{I}, \quad \alpha_2 = \mathbf{B}'^{2}_{\mathrm{d}}\cdot\mathbf{I}, \tag{18}$$

which satisfy the equations

$$\begin{aligned}\dot{\alpha_1} &= 2\,\mathrm{dev}\left(\mathbf{B}'_{\mathrm{d}}\right)\cdot\mathbf{D} - \Gamma\mathbf{A}_{\mathrm{d}}\cdot\mathbf{I},\\ \dot{\alpha_2} &= 4\,\mathrm{dev}\left(\mathbf{B}'^{2}_{\mathrm{d}}\right)\cdot\mathbf{D} - 2\Gamma\mathbf{A}_{\mathrm{d}}\cdot\mathbf{B}'_{\mathrm{d}}.\end{aligned} \tag{19}$$

The strain energy Σ_{d}, for elastically isotropic materials, is specified to be a function of $\{\alpha_1, \alpha_2\}$

$$\Sigma_{\mathrm{d}} = \Sigma_{\mathrm{d}}\left(\alpha_1, \alpha_2\right), \tag{20}$$

and the dissipative part $\boldsymbol{\sigma}_{\mathrm{d}}$ of the Cauchy stress is taken in the form

$$\boldsymbol{\sigma}_{\mathrm{d}} = \mathrm{dev}\left(\boldsymbol{\sigma}_{\mathrm{d}}\right) = 2\rho\frac{\partial\Sigma_{\mathrm{d}}}{\partial\alpha_1}\mathrm{dev}\left(\mathbf{B}'_{\mathrm{d}}\right) + 4\rho\frac{\partial\Sigma_{\mathrm{d}}}{\partial\alpha_2}\mathrm{dev}\left(\mathbf{B}'^{2}_{\mathrm{d}}\right). \tag{21}$$

Moreover, the rate of material dissipation (6) requires

$$\mathscr{D} = \Gamma\rho\left[\frac{\partial\Sigma_{\mathrm{d}}}{\partial\alpha_1}\mathbf{A}_{\mathrm{d}}\cdot\mathbf{I} + 2\frac{\partial\Sigma_{\mathrm{d}}}{\partial\alpha_2}\mathbf{A}_{\mathrm{d}}\cdot\mathbf{B}'_{\mathrm{d}}\right] \geqslant 0. \tag{22}$$

A model with a smooth elastic–inelastic transition which can be either rate-independent or rate-dependent, with and without a yield function is given by Hollenstein et al. [36]. For the model here considered, the value of Γ depends on the effective rate of total distortional deformation $\dot{\varepsilon}$ defined by

$$\dot{\varepsilon} = \sqrt{\frac{2}{3}\mathrm{dev}\left(\mathbf{D}\right)\cdot\mathrm{dev}\left(\mathbf{D}\right)}. \tag{23}$$

The experimental data of the *Manduca* muscle suggest that the functional form of Γ depends on the state of the dissipative component. In particular, a model is proposed for which the parameters $\{a, b\}$ have different values when the material is being loaded $\{a_{\mathrm{l}}, b_{\mathrm{l}}\}$ with the dissipative component being in a state of triaxial extension and when the material is being unloaded $\{a_{\mathrm{u}}, b_{\mathrm{u}}\}$ with the dissipative component being in a state of triaxial compression. Since data are only available for uniaxial stress, it is not possible to quantify a three-dimensional formulation that models all states of the dissipative component. Nevertheless, since the present model is developed for three-dimensional deformations, it is desirable to suggest a theoretical structure that can be used. To this end, it is recalled from Rubin [44] that simple isotropic functions can be developed using a Lode angle to distinguish between different states of the material. Motivated by this work, it is convenient to

introduce a Lode angle γ based on the deviatoric part of the elastic distortional deformation of the dissipative component by

$$\sin(3\gamma) = -\frac{27\det\left[\operatorname{dev}\left(\mathbf{B}'_{\mathrm{d}}\right)\right]}{2\left[\frac{3}{2}\operatorname{dev}\left(\mathbf{B}'_{\mathrm{d}}\right)\cdot\operatorname{dev}\left(\mathbf{B}'_{\mathrm{d}}\right)\right]^{3/2}}, \quad -\frac{\pi}{6}\leqslant\gamma\leqslant\frac{\pi}{6}. \tag{24}$$

Different functional forms of Γ were considered in [44], but here attention is limited to a Mohr–Coulomb-type model with Γ being specified by

$$\Gamma = a\left(a_{\mathrm{l}}, a_{\mathrm{u}}, \gamma\right) + b\left(b_{\mathrm{l}}, b_{\mathrm{u}}, \gamma\right)\dot{\varepsilon}, \tag{25}$$

where

$$a\left(a_{\mathrm{l}}, a_{\mathrm{u}}, \gamma\right) = \frac{\sqrt{3}\,a_{\mathrm{l}}\,a_{\mathrm{u}}}{\left(a_{\mathrm{l}}+a_{\mathrm{u}}\right)\cos\gamma + \sqrt{3}\left(a_{\mathrm{l}}-a_{\mathrm{u}}\right)\sin\gamma} > 0, \tag{26}$$

and

$$b\left(b_{\mathrm{l}}, b_{\mathrm{u}}, \gamma\right) = \frac{\sqrt{3}\,b_{\mathrm{l}}\,b_{\mathrm{u}}}{\left(b_{\mathrm{l}}+b_{\mathrm{u}}\right)\cos\gamma + \sqrt{3}\left(b_{\mathrm{l}}-b_{\mathrm{u}}\right)\sin\gamma} > 0, \tag{27}$$

and with $\{a_{\mathrm{l}}, a_{\mathrm{u}}, b_{\mathrm{l}}, b_{\mathrm{u}}\}$ being positive constants. This functional dependence of Γ on the Lode angle γ can be modified once multi-axial data become available.

For the simple case of uniaxial stress in the fixed unit $\mathbf{s}$ direction, starting from zero stress in the dissipative component, the distortional deformation tensor $\mathbf{B}'_{\mathrm{d}}$ can be written as a function of the stretch $\lambda_{\mathrm{d}} > 0$ in the form

$$\mathbf{B}'_{\mathrm{d}} = \lambda_{\mathrm{d}}^2\,\mathbf{s}\otimes\mathbf{s} + \frac{1}{\lambda_{\mathrm{d}}}\left(\mathbf{I}-\mathbf{s}\otimes\mathbf{s}\right), \quad \mathbf{s}\cdot\mathbf{s} = 1. \tag{28}$$

It can be shown that

$$\gamma = -\frac{\pi}{6}, \quad a\left(a_{\mathrm{l}}, a_{\mathrm{u}}, -\frac{\pi}{6}\right) = a_{\mathrm{l}}, \quad b\left(b_{\mathrm{l}}, b_{\mathrm{u}}, -\frac{\pi}{6}\right) = b_{\mathrm{l}} \quad \text{for} \quad \lambda_{\mathrm{d}} > 1, \tag{29}$$

$$\gamma = \frac{\pi}{6}, \quad a\left(a_{\mathrm{l}}, a_{\mathrm{u}}, \frac{\pi}{6}\right) = a_{\mathrm{u}}, \quad b\left(b_{\mathrm{l}}, b_{\mathrm{u}}, \frac{\pi}{6}\right) = b_{\mathrm{u}} \quad \text{for} \quad \lambda_{\mathrm{d}} < 1. \tag{30}$$

Thus, the values $\{a_{\mathrm{l}}, b_{\mathrm{l}}\}$ characterize loading with the dissipative component being in triaxial extension $\{\lambda_{\mathrm{d}} > 1\}$ and the values $\{a_{\mathrm{u}}, b_{\mathrm{u}}\}$ characterize unloading with the dissipative component in triaxial compression $\{\lambda_{\mathrm{d}} < 1\}$.

4 Robust, strongly objective numerical integration algorithm

A robust, strongly objective numerical integration algorithm was developed in Hollenstein et al. [36], which can be applied to the evolution Eqs. (7), (8) and (16). This algorithm is briefly summarized in this section with reference to the proposed model. Specifically, it is assumed that at time $t = t_1$ the values $\{J(t_1), \mathbf{B}'(t_1), \mathbf{B}'_{\mathrm{d}}(t_1)\}$ of $\{J, \mathbf{B}', \mathbf{B}'_{\mathrm{d}}\}$ are known and the objective is to find the values $\{J(t_2), \mathbf{B}'(t_2), \mathbf{B}'_{\mathrm{d}}(t_2)\}$ of these quantities at the end of the time step at $t = t_2$ with $\Delta t = t_2 - t_1$.

Following the work in [45–47], it is convenient to define the relative deformation gradient $\mathbf{F}_{\mathrm{r}}$, the relative dilatation J_{r} and the unimodular part $\mathbf{F}'_{\mathrm{r}}$ of $\mathbf{F}_{\mathrm{r}}$ by the evolution equations

$$\dot{\mathbf{F}}_{\mathrm{r}} = \mathbf{L}\mathbf{F}_{\mathrm{r}}, \quad \dot{J}_{\mathrm{r}} = J_{\mathrm{r}}\mathbf{D}\cdot\mathbf{I}, \quad \dot{\mathbf{F}}'_{\mathrm{r}} = \mathbf{L}\mathbf{F}'_{\mathrm{r}} - \frac{1}{3}\left(\mathbf{D}\cdot\mathbf{I}\right)\mathbf{F}'_{\mathrm{r}}, \tag{31}$$

with the initial conditions

$$\mathbf{F}_{\mathrm{r}}\left(t_1\right) = \mathbf{I}, \quad J_{\mathrm{r}}\left(t_1\right) = 1, \quad \mathbf{F}'_{\mathrm{r}}\left(t_1\right) = \mathbf{I}, \tag{32}$$

where

$$J_{\mathrm{r}} = \det\left(\mathbf{F}_{\mathrm{r}}\right), \quad \mathbf{F}'_{\mathrm{r}} = J_{\mathrm{r}}^{-1/3}\mathbf{F}_{\mathrm{r}}. \tag{33}$$

For finite element programs, the value $\mathbf{F}_{\mathrm{r}}(t_2)$ can be determined directly in terms of the nodal displacements during the time step so that the evolution Eqs. (31) and (32) do not need to be integrated explicitly.

Now, the exact solutions of (7) and (8) can be written in the forms

$$J(t_2) = J_{\mathrm{r}}(t_2)\, J(t_1)\,, \quad \mathbf{B}'(t_2) = \mathbf{F}'_{\mathrm{r}}(t_2)\, \mathbf{B}'(t_1)\, \mathbf{F}'^{\mathrm{T}}_{\mathrm{r}}(t_2)\,. \tag{34}$$

Also, the elastic trial value of $\mathbf{B}'_{\mathrm{d}}$, denoted by $\mathbf{B}'^{\star}_{\mathrm{d}}$, determined by the solution of (16) with vanishing rate of inelastic deformation $\Gamma = 0$, can be expressed in the form

$$\mathbf{B}'^{\star}_{\mathrm{d}} = \mathbf{F}'_{\mathrm{r}}(t_2)\, \mathbf{B}'_{\mathrm{d}}(t_1)\, \mathbf{F}'^{\mathrm{T}}_{\mathrm{r}}(t_2)\,. \tag{35}$$

Using an implicit backward Euler integrated approximation, the auxiliary tensor $\bar{\mathbf{B}}'_{\mathrm{d}} \approx \mathbf{B}'_{\mathrm{d}}(t_2)$ associated with the evolution Eq. (16) is given by

$$\bar{\mathbf{B}}'_{\mathrm{d}} = \mathbf{B}'^{\star}_{\mathrm{d}} - \Delta t \Gamma(t_2) \left[\bar{\mathbf{B}}'_{\mathrm{d}} - \left(\frac{3}{\bar{\mathbf{B}}'^{-1}_{\mathrm{d}} \cdot \mathbf{I}} \right) \mathbf{I} \right], \tag{36}$$

where $\Gamma(t_2)$ is the value of Γ at the end of the time step. Next, taking the deviatoric part of (36) and requiring that $\mathrm{dev}\left[\mathbf{B}'_{\mathrm{d}}(t_2)\right] = \mathrm{dev}\left(\bar{\mathbf{B}}'_{\mathrm{d}}\right)$ it follows that

$$\mathrm{dev}\left[\mathbf{B}'_{\mathrm{d}}(t_2)\right] = \frac{1}{1 + \Delta t \Gamma(t_2)} \mathrm{dev}\left(\mathbf{B}'^{\star}_{\mathrm{d}}\right). \tag{37}$$

In order to determine the value of $\Gamma(t_2)$ in (37), it is recalled from Papes [48] that the value $\bar{\mathbf{D}}$ of $\mathbf{D}(t_2)$ at the end of the time step can be approximated by

$$\mathbf{D}(t_2) \approx \bar{\mathbf{D}} = \frac{1}{2\Delta t} \left[\mathbf{F}_{\mathrm{r}}(t_2)\, \mathbf{F}^{\mathrm{T}}_{\mathrm{r}}(t_2) - \mathbf{I} \right], \tag{38}$$

so that the average increment of the effective total rate of deformation, defined in (23), can be approximated by

$$\Delta\varepsilon = \Delta t\, \dot{\varepsilon}(t_2) \approx \Delta t \sqrt{\frac{2}{3} \mathrm{dev}\left(\bar{\mathbf{D}}\right) \cdot \mathrm{dev}\left(\bar{\mathbf{D}}\right)} \tag{39}$$

and the Lode angle γ in (24) is given by

$$\sin(3\gamma) = -\frac{27 \det\left[\mathrm{dev}\left(\bar{\mathbf{D}}\right)\right]}{2\left[\frac{3}{2}\mathrm{dev}\left(\bar{\mathbf{D}}\right) \cdot \mathrm{dev}\left(\bar{\mathbf{D}}\right)\right]^{3/2}}, \quad -\frac{\pi}{6} \leqslant \gamma \leqslant \frac{\pi}{6}. \tag{40}$$

Thus, $\Delta t \Gamma(t_2)$ becomes

$$\Delta t \Gamma(t_2) = \Delta t\, a(a_{\mathrm{l}}, a_{\mathrm{u}}, \gamma) + b(b_{\mathrm{l}}, b_{\mathrm{u}}, \gamma)\ \Delta\varepsilon. \tag{41}$$

Finally, using (41) in (37), the value of $\mathbf{B}'_{\mathrm{d}}$ at the end of the time step can be expressed in the form

$$\mathbf{B}'_{\mathrm{d}}(t_2) = \mathrm{dev}\left[\mathbf{B}'_{\mathrm{d}}(t_2)\right] + \frac{1}{3}\alpha(t_2)\, \mathbf{I}, \tag{42}$$

where the scalar $\alpha(t_2)$ is determined by solving the cubic equation

$$\det\left[\mathbf{B}'_{\mathrm{d}}(t_2)\right] = 1. \tag{43}$$

For details, see Eq. (49a) in Rubin and Attia [43].

5 Specific constitutive equations

Since many soft tissues experience large distortional deformations relative to volumetric deformations, it is convenient to consider them to be incompressible by introducing the volumetric constraint

$$J = 1. \tag{44}$$

The constraint response that enforces the incompressibility condition (44) effectively replaces the pressure p_{e} in (13) by an arbitrary function that is determined by the balance of linear momentum and boundary conditions. It follows that only the distortional response of the strain energy function Σ_e needs to be specified. Specifically, here Σ_e is taken in the form

$$\rho_0 \Sigma_{\mathrm{e}} = \frac{\mu_{\mathrm{e}}}{2\beta_{\mathrm{e}}} \left\{ \exp\left[\beta_{\mathrm{e}}(\beta_1 - 3)\right] - 1 \right\}, \tag{45}$$

where μ_e is a nonnegative, constant shear modulus and β_e is a positive material constant that controls the nonlinearity of the elastic response. Then, using (14) the elastic part $\boldsymbol{\sigma}_{\mathrm{e}}$ of the stress is given by

$$\boldsymbol{\sigma}_{\mathrm{e}} = -p_{\mathrm{e}}\mathbf{I} + \mu_{\mathrm{e}} \exp\left[\beta_{\mathrm{e}}\left(\beta_1 - 3\right)\right] \operatorname{dev}\left(\mathbf{B}'\right). \tag{46}$$

The constitutive equation for the elastic strain energy of the dissipative component is taken in a similar form to (45) with

$$\rho_0 \Sigma_{\mathrm{d}} = \frac{\mu_{\mathrm{d}}}{2\alpha_{\mathrm{d}}} \left\{ \exp\left[\alpha_{\mathrm{d}}(\alpha_1 - 3)\right] - 1 \right\}, \tag{47}$$

where μ_{d} is a nonnegative, constant shear modulus and α_{d} is a positive material constant that controls nonlinearity of the elastic response of the dissipative component. It then follows from (21) that the dissipative part $\boldsymbol{\sigma}_{\mathrm{d}}$ of the stress is given by

$$\boldsymbol{\sigma}_{\mathrm{d}} = \operatorname{dev}\left(\boldsymbol{\sigma}_{\mathrm{d}}\right) = \mu_{\mathrm{d}} \exp\left[\alpha_{\mathrm{d}}\left(\alpha_1 - 3\right)\right] \operatorname{dev}\left(\mathbf{B}'_{\mathrm{d}}\right). \tag{48}$$

Also, the rate of material dissipation (22) requires

$$\mathscr{D} = \frac{1}{2}\Gamma \mu_{\mathrm{d}} \exp\left[\alpha_{\mathrm{d}}\left(\alpha_1 - 3\right)\right] \left(\mathbf{A}_{\mathrm{d}} \cdot \mathbf{I}\right) \geqslant 0. \tag{49}$$

It can be shown that by expressing $\mathbf{B}'_{\mathrm{d}}$ in its spectral form that the expression $\mathbf{A}_{\mathrm{d}} \cdot \mathbf{I}$ is nonnegative so that (49) is satisfied by the functional form (25) for Γ.

6 Simulation

The model developed in the previous sections is used here to simulate the experimental data for simple uniaxial tension of the *Manduca* muscle. To this end, λ is taken to be the axial stretch in the fixed $\mathbf{s}$ direction with the material being stress-free in its initial state with

$$\lambda(0) = 1, \quad \mathbf{B}'(0) = \mathbf{I}, \quad \mathbf{B}'_{\mathrm{d}}(0) = \mathbf{I}. \tag{50}$$

Moreover, the velocity gradient $\mathbf{L}$ is specified by (28) so that the solutions of the evolution equations (8) and (16) give

$$\mathbf{B}' = \lambda^2 \mathbf{s} \otimes \mathbf{s} + \frac{1}{\lambda}\left(\mathbf{I} - \mathbf{s} \otimes \mathbf{s}\right), \quad \beta_1 = \frac{\lambda^3 + 2}{\lambda}, \tag{51}$$

$$\mathbf{B}'_{\mathrm{d}} = \lambda_{\mathrm{d}}^2 \mathbf{s} \otimes \mathbf{s} + \frac{1}{\lambda_{\mathrm{d}}}\left(\mathbf{I} - \mathbf{s} \otimes \mathbf{s}\right), \quad \alpha_1 = \frac{\lambda_{\mathrm{d}}^3 + 2}{\lambda_{\mathrm{d}}}, \tag{52}$$

where λ_{d} is the stretch associated with the dissipative component. Thus, for uniaxial stress in the $\mathbf{s}$ direction, the pressure p_e is determined by the condition that the lateral stress vanishes. The total stress is represented in the form

$$\boldsymbol{\sigma} = \sigma \mathbf{s} \otimes \mathbf{s}, \tag{53}$$

where the explicit expression for σ, using (4), (46) and (48), is given by

$$\sigma = \mu_{\mathrm{e}} \exp\left[\beta_{\mathrm{e}} \left(\beta_1 - 3\right)\right] \left(\lambda^2 - \frac{1}{\lambda}\right) + \mu_{\mathrm{d}} \exp\left[\alpha_{\mathrm{d}} \left(\alpha_1 - 3\right)\right] \left(\lambda_{\mathrm{d}}^2 - \frac{1}{\lambda_{\mathrm{d}}}\right). \tag{54}$$

Furthermore, for incompressible material subject to simple uniaxial tension, the nominal axial stress Π (stress per unit reference area) is given by

$$\Pi = \frac{\sigma}{\lambda}. \tag{55}$$

Now, using the numerical procedure described in Sect. 4, it follows that the value of the unimodular part of the relative deformation gradient at the end of a typical time step, $\mathbf{F}_{\mathrm{r}}' \left(t_2\right)$, is given by

$$\mathbf{F}_{\mathrm{r}}' \left(t_2\right) = \frac{\lambda \left(t_2\right)}{\lambda \left(t_1\right)} \mathbf{s} \otimes \mathbf{s} + \sqrt{\frac{\lambda \left(t_1\right)}{\lambda \left(t_2\right)}} \left(\mathbf{I} - \mathbf{s} \otimes \mathbf{s}\right), \tag{56}$$

and the elastic trial value $\lambda_d^{\star}$ of λ_d can be expressed by

$$\lambda_{\mathrm{d}}^{\star} = \left[\frac{\lambda \left(t_2\right)}{\lambda \left(t_1\right)}\right] \lambda_d \left(t_1\right). \tag{57}$$

Then, Eq. (37) yields a cubic equation for $\lambda_{\mathrm{d}} \left(t_2\right)$ in the form

$$\lambda_{\mathrm{d}}^2 \left(t_2\right) - \frac{1}{\lambda_{\mathrm{d}} \left(t_2\right)} = \left[\frac{1}{1 + \Delta t \Gamma \left(t_2\right)}\right] \left(\lambda_{\mathrm{d}}^{\star 2} - \frac{1}{\lambda_{\mathrm{d}}^{\star}}\right). \tag{58}$$

Moreover, in determining the value of $\Gamma \left(t_2\right)$ in (41) use has been made of the expression (38), which yields

$$\mathrm{dev}\left(\bar{\mathbf{D}}\right) = \frac{1}{2\Delta t} \left[\frac{\lambda^2 \left(t_2\right)}{\lambda^2 \left(t_1\right)} - \frac{\lambda \left(t_1\right)}{\lambda \left(t_2\right)}\right] \left(\mathbf{s} \otimes \mathbf{s} - \frac{1}{3}\mathbf{I}\right). \tag{59}$$

Then, using the values $\{\lambda \left(t_2\right), \lambda_{\mathrm{d}} \left(t_2\right)\}$ together with (51)–(55) gives the value of the nominal stress $\Pi \left(t_2\right)$ at the end of the time step.

7 Model predictions

The rate-dependent response of an unstimulated muscle, the recovery of muscle properties from the preconditioned state and stress relaxation for constant stretches are now evaluated using the formulation presented in Sect. 5. Recordings of experimental data were initiated when the stretch $\lambda = \lambda_{\mathrm{r}}$ corresponding to the resting length of the muscle. For completeness, the numerical computation includes the stress-free initial state and a quasi-static extension from $\lambda(0) = 1$ to $\lambda_{\mathrm{r}} = 1.05$, which ensures zero stress in the dissipative component. At $\lambda = \lambda_{\mathrm{r}}$, the stretch rate changes and assumes values equivalent to those used in the experimental characterization. The data shown in Figs. 2, 3 and 4 are obtained from different muscles so that due to the variability of biological tissue, a change in the material parameters should be expected. This is shown by comparing values of corresponding parameters in Tables 1, 2 and 3. Trial and error estimates are used to determine the parameters μ_{e} and β_{e} of the elastic energy function (45). The remaining parameters, $\{\mu_{\mathrm{d}}, \alpha_{\mathrm{d}}\}$ used to define the energy Σ_{d} in (47) and $\{a_{\mathrm{l}}, b_{\mathrm{l}}, a_{\mathrm{u}}, b_{\mathrm{u}}\}$ to define Γ in (25), are determined by a least square optimization routine using the data shown in Sect. 2.

Table 1 Model parameters used to simulate the rate-dependent response of an unstimulated muscle

μ_e	β_e	μ_d	α_d	a_l	b_l	a_u	b_u
0.06	5	0.16	6	0.16	8	0.6	60

The values of a_l and a_u are in s^{-1} and μ_e and μ_d are given in MPa

Table 2 Magnitudes of the material model parameters used to simulate the recovery of passive muscle properties from a preconditioned state

μ_e	β_e	μ_d	α_d	a_l	b_l	a_u	b_u
0.17	3.9	0.31	2.3	0.25	12	0.3	40

The values of a_l and a_u are in s^{-1} and the μ_e and μ_d are given in MPa

Table 3 Summary of material model parameters describing stress relaxation of an unstimulated muscle during loading and unloading in simple tension

μ_e	β_e	μ_d	α_d	a_l	b_l	a_u	b_u
0.06	5.5	0.22	11	0.04	6.5	1	80

The values of a_l and a_u are in s^{-1} and the μ_e and μ_d are given in MPa

7.1 Rate-dependent response

Figure 2 summarizes experimental data of the rate-dependent response of an unstimulated *Manduca* muscle for stretch rates $\dot{\lambda} = 0.0144, 0.072, 0.36$ and $1.8\ s^{-1}$. These data are used to determine the corresponding material model parameters, which are summarized in Table 1 and used to obtain the numerical results depicted in Fig. 5. Specifically, the numerical results show the nominal stress Π as a function of the stretch λ for two loading–unloading cycles in simple tension with maximum extension $\lambda = 1.24$ for $\dot{\lambda} = 0.0144, 0.072, 0.36$ and $1.8\ s^{-1}$. The results also show a change in material response when transitioning from quasi-static loading to the specified stretch rate at $\lambda = \lambda_r$. The inelastic behavior is characterized by the permanent set of the material at completion of the first loading–unloading cycle. Reloading differs from the primary loading path indicating preconditioning of the material similar to the Mullins effect observed in rubberlike materials [49–51]. For convenience of comparison, experimental behavior for loading–unloading cycles of the preconditioned material are included as dashed curves in Fig. 5. Comparing the numerical results with the experimental data validates the formulation of the proposed model to simulate the rate-dependent response of *Manduca* muscle.

7.2 Recovery from preconditioned state

The material model is now used to describe the time-dependent recovery of a *Manduca* muscle from the preconditioned state. The experimental data in Fig. 3 show three loading–unloading cycles at constant strain rate and maximum extension $\lambda = 1.24$. At the end of each unloading, the muscle is held at the resting length for three minutes during which the material nearly recovers its prestressed resting state. These data are now used to determine material parameters, which are summarized in Table 2 with the corresponding numerical results given in Fig. 6. The graph on the left starts from the stress-free configuration $\lambda(0) = 1$ and shows the nominal stress Π as a function of λ for three loading–unloading cycles. The transition from quasi-static loading to the stretch rate $\dot{\lambda} = 0.18\ s^{-1}$ is again visible during primary loading when $\lambda = \lambda_r$. During unloading, the material does not return to the initial stress-free state clearly showing the inelastic component of the deformation. During the recovery time, at constant stretch $\lambda = \lambda_r$, the stress increases but does not reach the primary loading state. Therefore, the reloading again differs from primarily loading. The nominal stress Π as a function of time is shown in the graph on the right in Fig. 6. Experimental behavior, depicted by dashed curves, is included to assess the accuracy of the model prediction.

7.3 Stress relaxation

The data in Fig. 4 are used to determine a set of material parameters that represent the time-dependent response of the *Manduca* muscle used in this study. These are listed in Table 3 and are used to simulate stress relaxation

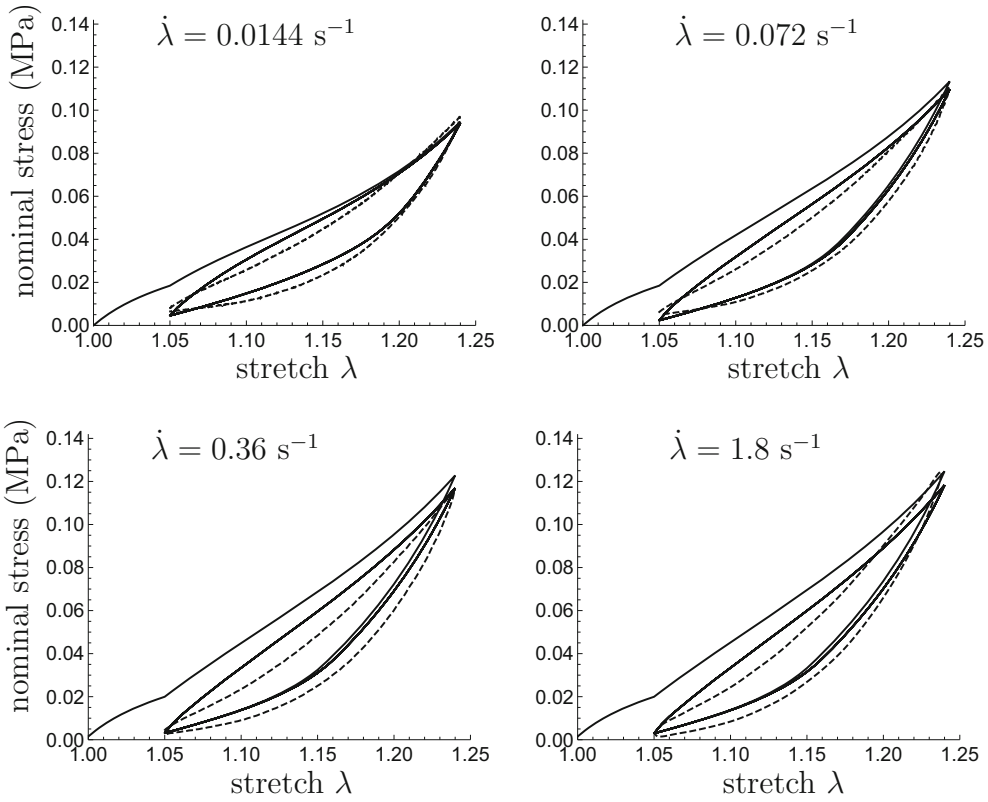

Fig. 5 Numerical results showing two loading–unloading cycles of an unstimulated *Manduca* muscle in simple tension with maximum extension $\lambda = 1.24$ and stretch rates of $\dot{\lambda} = 0.0144\ \mathrm{s}^{-1}$, $\dot{\lambda} = 0.072\ \mathrm{s}^{-1}$, $\dot{\lambda} = 0.36\ \mathrm{s}^{-1}$ and $\dot{\lambda} = 1.8\ \mathrm{s}^{-1}$. The *dashed curves* represent the experimental behavior of the preconditioned material. All graphs depict the nominal stress as a function of the stretch λ

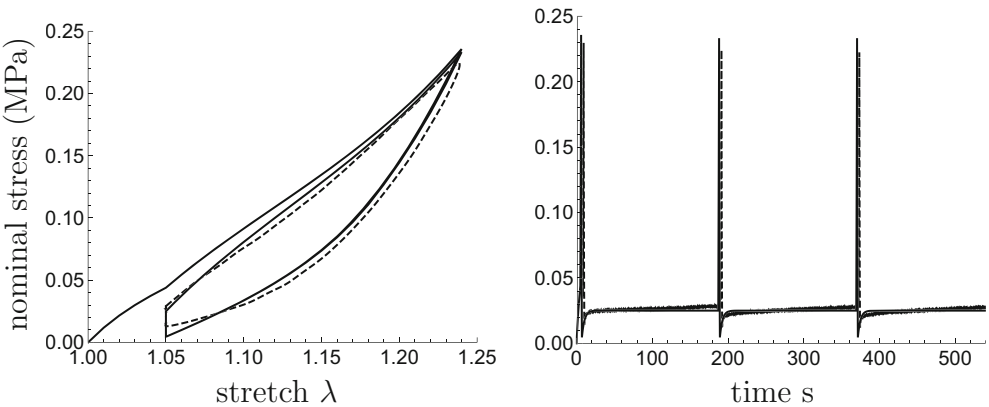

Fig. 6 Numerical results representing three loading–unloading cycles of an unstimulated muscle in simple tension. At the end of each cycle, at the resting length $\lambda_r = 1.05$, a 180 s recovery period is included to allow recovery of muscle properties from the preconditioned state. The graph on the *left* shows the loading–unloading response, and the graph on the *right* depicts the change in nominal stress as a function of time. The *dashed curves* represent the experimental behavior of the preconditioned material. Experimental data in Fig. 3 show that the stress-stretch response of the preconditioned muscle coincides during the second and third loading cycles. Therefore, for clarity of representation, only one loading–unloading cycle is included in the graph on the *left*

at constant stretch during loading and unloading portions of a cycle of simple uniaxial tension. Figure 7 shows the numerical results of an unstimulated muscle in simple tension from the stress-free configuration $\lambda(0) = 1$ to a maximum stretch $\lambda \approx 1.25$. The loading rate changes from quasi-static to $\dot{\lambda} = 0.2\ \mathrm{s}^{-1}$ at $\lambda_r = 1.05$. During loading and unloading, portions of the cycle the stretch are held constant for 30 seconds at $\lambda = 1.12$ and $\lambda = 1.19$ and the change in stress as a function of time is evaluated numerically. The change of the

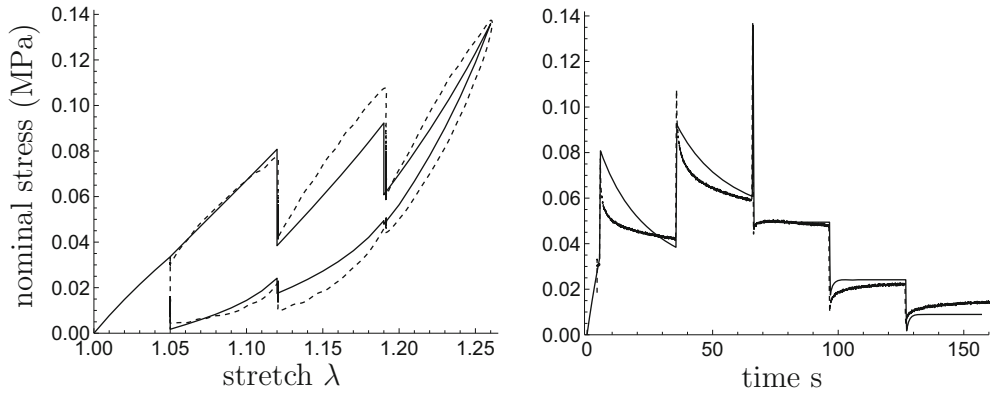

Fig. 7 Numerical results showing the response of the unstimulated *Manduca* muscle in simple tension. The graph on the *left* shows the nominal stress versus stretch during loading and unloading. The graph on the *right* depicts stress relaxation as a function of time for constant values of λ. Experimental behavior, depicted by the *dashed curves*, is included to assess the accuracy of the model prediction

nominal stress Π with time, depicted in the graph on the right in Fig. 7, differs from that during loading and unloading portions of the cycle. Specifically, during loading the stress decays with relaxation not completed after 30 seconds and during unloading the stress increases reaching a constant value in less than 30 seconds. This requires different values of the material parameters $\{a, b\}$ to define Γ during loading and unloading, see Eq. (25). The graph on the right shows a change in slope at $t = 5$ s indicating the change in loading rate at $\lambda = \lambda_r$. The dashed curves in Fig. 7 represent the observed behavior and are used to quantify the accuracy of the numerical prediction.

8 Discussion and concluding remarks

Motivated by the need to characterize the time-dependent response of skeletal muscle, this paper presents new experimental data and a phenomenological constitutive model that captures the observed behavior with reasonable accuracy. The data, from the unstimulated ventral interior lateral muscle of the third abdominal segment of *Manduca sexta*, are limited to simple uniaxial tensile loading–unloading in the fiber direction. The experimental characterization quantifies the inelastic rate-dependent behavior, the recovery of muscle properties from the preconditioned response toward the prestressed resting state and stress relaxation at constant stretch during loading and unloading.

The proposed model considers the material as a composite of a nonlinear hyperelastic component in parallel with a dissipative component. In contrast to standard nonlinear inelastic models, here the dissipative component is modeled using an evolution equation that combines rate-independent and rate-dependent behavior, which exhibits smooth response with no finite elastic range. The three-dimensional constitutive model is specialized to simple uniaxial tension in the preferred direction; hence, an isotropic formulation provides sufficient flexibility to capture the mechanical response. As such, the structure of the proposed formulation is not muscle specific, i.e., a change in the material parameters fully accounts for the variability of biological tissue. The restriction imposed by the current isotropic formulation is that the principal direction of the uniaxial stress component and the preferred direction of the material coincide.

Acknowledgments This research was supported by the National Science Foundation (Grant Nos. CMMI-1031366, CMMI-1352955 and IOS-1050908) and by a Faculty Research Award provided by Tufts University. This research was partially supported by MB Rubin's Gerard Swope Chair in Mechanics.

References

1. Paetsch, C., Trimmer, B.A., Dorfmann, A.: A constitutive model for active-passive transition of muscle fibers. Int. J. Nonlinear Mech. **47**, 377–387 (2012)
2. Paetsch, C., Dorfmann, A.: Non-linear modeling of active biohybrid materials. Int. J. Nonlinear Mech. **56**, 105–114 (2013)
3. Paetsch, C., Dorfmann, L.: Stability of active muscle tissue. J. Eng. Math. (2015). doi:10.1007/s10665-014-9750-1

4. Dorfmann, A., Trimmer, B.A., Woods, W.A.: A constitutive model for muscle properties in a soft-bodied arthropod. J. R. Soc. Interface **4**, 257–269 (2007)
5. Wineman, A.S., Rajagopal, K.R.: Mechanical response of polymers. Cambridge Press, Cambridge (2000)
6. Christensen, R.M.: Theory of viscoelasticty. Dover, NY (1982)
7. Proske, U., Morgan, D.L.: Do cross-bridges contribute to the tension during stretch of passive muscle? J. Muscle Res. Cell Motil. **20**, 433–442 (1999)
8. Mutungi, G., Ranatunga, K.W.: Do cross-bridges contribute to the tension during stretch of passive muscle? A response J. Muscle Res. Cell Motil. **21**, 301–302 (2000)
9. Bagni, M.A., Colombini, B., Geiger, P., Berlinguer Palmini, R., Cecchi, G.: Non-cross-bridge calcium-dependent stiffness in frog muscle fibers J. Physiol. Lond. **286**, 1353–1357 (2004)
10. Campbell, K.S., Lakie, M.: A cross-bridge mechanism can explain the thixotropic short-range elastic component of relaxed frog skeletal muscle J. Physiol. Lond. **510**, 941–962 (1998)
11. Granzier, H.L., Labeit, S.: The giant protein titin: a major player in myocardial mechanics, signaling, and disease Circ. Res. **94**, 284–295 (2004)
12. Granzier, H.L., Wang, K.: Interplay between passive tension and strong and weak binding cross-bridges in insect indirect flight muscle. A functional dissection by gelsolin-mediated thin filament removal J. Gen. Physiol. **101**, 235–270 (1993)
13. Granzier, H.L., Wang, K.: Passive tension and stiffness of vertebrate skeletal and insect flight muscles: The contribution of weak cross-bridges and elastic filaments Biophys. J. **65**, 2141–2159 (1993)
14. Gosline, J., Lillie, M., Carrington, E., Guerette, P., Ortlepp, C., Savage, K.: Elastic proteins: Biological roles and mechanical properties Philos. Trans. R. Soc. Lond. B **357**, 121–132 (2002)
15. Lieber, R.L., Leonard, M.E., Brown-Maupin, C.G.: Effects of muscle contraction on the load-strain properties of frog aponeurosis and tendon Cells Tissues Organs **166**, 48–54 (2000)
16. Powers, K., Schappacher-Tilp, G., JinhaA. Leonard, T., Nishikawa, K., Herzog, W.: Titin force is enhanced in actively stretched skeletal muscle J. Exp. Biol. **217**, 3629–3636 (2014)
17. Gautel, M.: The sarcomeric cytoskeleton: who picks up the strain? Curr. Opin. Cell Biol. **23**, 39–46 (2011)
18. Ortega, J.O., Lindstedt, S.L., Nelson, F.E., Jubrias, S.A., Kushmerick, M.J., Conley, K.E.: Muscle force, work and cost: a novel technique to revisit the Fenn effect. J. Exp. Biol. doi:10.1242/jeb114512 (2015)
19. Hill, A.V.: The heat of shortening and the dynamic constants of muscle Proc. R. Soc. Lond. B **126**, 136–195 (1938)
20. Martins, J.A.C., Pires, E.B., Salvado, R., Dinis, P.B.: A numerical model of passive and active behavior of skeletal muscles Comput. Methods Appl. Mech. Eng. **151**, 419–433 (1998)
21. Parente, M.P.L., Natal Jorge, R.M., Mascarenhas, T., Fernandes, A.A., Martins, J.A.C.: The influence of the material properties on the biomechanical behavior of the pelvic floor muscles during vaginal delivery J. Biomech. **42**, 1301–1306 (2009)
22. Tang, C.Y., Zhang, G., Tsui, C.P.: A 3D skeletal muscle model coupled with active contraction of muscle fibres and hyperelastic behavior J. Biomech. **126**, 865–872 (2009)
23. Palevski, A., Glaich, I., Portnoy, S., Linder-Ganz, E., Gefen, A.: Stress relaxation of porcine gluteus muscle subjected to sudden transverse deformation as related to pressure sore modeling J. Biomech. **128**, 782–787 (2006)
24. Van Loocke, M., Lyons, C.G., Simms, C.K.: Viscoelastic properties of passive skeletal muscle in compression: stress-relaxation behaviour and constitutive modelling J. Biomech. **41**, 1555–1566 (2008)
25. Meyer, G.A., McCulloch, A.D., Lieber, R.L.: A nonlinear model of passive muscle viscosity J. Appl. Mech. Trans. ASME **133(091007)**, 1–9 (2011)
26. Rehorn, M.R., Schroer, A.K., Blemker, S.S.: The passive properties of muscle fibers are velocity dependent J. Biomech. **47**, 687–693 (2014)
27. Bosboom, E.M.H., Hesselink, M.K.C., Oomens, C.W.J., Bouten, C.V.C., Drost, M.R., Baaijens, F.P.T.: Passive transverse mechanical properties of skeletal muscle under in vivo compression J. Biomech. **34**, 1365–1368 (2001)
28. Van Loocke, M., Lyons, C.G., Simms, C.K.: A validated model of passive muscle in compression J. Biomech. **39**, 2999–3009 (2006)
29. Van Loocke, M., Lyons, C.G., Simms, C.K.: Viscoelastic properties of passive skeletal muscle in compression: Cyclic behaviour J. Biomech. **42**, 1038–1048 (2009)
30. Röhrle, O., Pullan, A.J.: Three-dimensional finite element modelling of muscle forces during mastication J. Biomech. **40**, 3363–3372 (2007)
31. Ito, D., Tanaka, E., Yamamoto, S.: A novel constitutive model of skeletal muscle taking into account anisotropic damage J. Mech. Behav. Biomed. Mater. **3**, 85–93 (2010)
32. Lu, Y.T., Zhu, H.X., Richmond, S., Middleton, J.: A visco-hyperelastic model for skeletal muscle tissue under high strain rates J. Biomech. **43**, 2629–2632 (2010)
33. Calvo, B., Sierra, M., Grasa, J., Mu noz, M.J., Pe na, E.: Determination of passive viscoelastic response of the abdominal muscle and related constitutive modeling: stress-relaxation behavior J. Mech. Behav. Biomed. Mat. **36**, 47–58 (2014)
34. Dorfmann, A.L., Woods, W.A., Trimmer, B.A.: Muscle performance in a soft-bodied terrestrial crawler: constitutive modeling of strain-rate dependency J. R. Soc. Interface **5**, 349–362 (2008)
35. Hunter, P.J., McCulloch, A.D., ter Keurs, H.E.D.J.: Modelling the mechanical properties of cardiac muscle Prog. Biophys. Mol. Biol. **69**, 289–331 (1998)
36. Hollenstein, M., Jabareen, M., Rubin, M.B.: Modeling a smooth elastic-inelastic transition with a strongly objective numerical integrator needing no iteration Comput. Mech. **52**, 649–667 (2013)
37. Perzyna, P.: The constitutive equations for rate sensitive plastic materials Q. Appl. Math. **20**, 321–332 (1963)
38. Lubliner, L., Taylor, R.L., Auricchio, F.: A new model of generalized plasticity and its numerical implementation Int. J. Solids Struct. **30**, 3171–3184 (1993)
39. Panoskaltsis, V.P., Polymenakos, L.C., Soldatos, D.: On large deformation generalized plasticity J. Mech. Mater. Struct. **3**, 441–457 (2008)
40. Einav, I.: The unification of hypoplastic and elasto-plastic theories Int. J. Solids Struct. **49**, 1305–1315 (2012)
41. Flory, P.J.: Thermodynamic relations for highly elastic materials Trans. Faraday Soc. **57**, 829–838 (1961)

42. Ogden, R.W.: Nearly isochoric elastic deformations: application to rubberlike solids J. Mech. Phys. Solids **26**, 37–57 (1978)
43. Rubin, M.B., Attia, A.: Calculation of hyperelastic response of finitely deformed elastic-viscoplastic materials Int. J. Numer. Methods Eng. **39**, 309–320 (1996)
44. Rubin, M.B.: A simple and convenient isotropic failure surface ASCE J. Eng. Mech. **117**, 348–369 (1991)
45. Rubin, M.B., Papes, O.: Advantages of formulating evolution equations for elastic-viscoplastic materials in terms of the velocity gradient instead of the spin tensor J. Mech. Mater. Struct. **6**, 529–543 (2011)
46. Simo, J.C.: Algorithms for static and dynamic multiplicative plasticity that preserve the classical return mapping schemes of the infinitesimal theory Comput. Methods Appl. Mech. Eng. **99**, 61–112 (1992)
47. Simo, J.C., Hughes, T.J.R.: Computational inelasticity. Springer, New York (1998)
48. Papes, O.: Nonlinear continuum mechanics in engineering applications. Ph. D. dissertation DISS ETH NO 19956, ETH Zurich (2012)
49. Dorfmann, A., Ogden, R.W.: A pseudo-elastic model for loading, partial unloading and reloading of particle-reinforced rubber Int. J. Solids Struct. **40**, 2699–2714 (2003)
50. Dorfmann, A., Ogden, R.W.: A constitutive model for the Mullins effect with permanent set in particle-reinforced rubber Int. J. Solids Struct. **41**, 1855–1878 (2004)
51. Dorfmann, A., Pancheri, F.Q.: A constitutive model for the Mullins effect with changes in material symmetry Int. J. Nonlin. Mech. **47**, 874–887 (2012)